Vol. 6, No. 3, June 2022, pp. 244-251

Current Optics and Photonics

Regular Paper

Spectral Reconstruction for High Spectral Resolution in a Static Modulated Fourier-transform Spectrometer

Ju Yong Cho[1], Seunghoon Lee[2], Hyoungjin Kim[1], and Won Kweon Jang[1]*

[1]*Department of Aeronautic Electricity, Hanseo University, Seosan 31962, Korea*
[2]*Satellite Research Directorate, Korea Aerospace Research Institute, Daejeon 34133, Korea*

(Received December 6, 2021 : revised March 15, 2022 : accepted March 22, 2022)

We introduce a spectral reconstruction method to enhance the spectral resolution in a static modulated Fourier-transform spectrometer. The optical-path difference and the interferogram in the focal plane, as well as the relationship of the interferogram and the spectrum, are discussed. Additionally, for better spectral reconstruction, applications of phase-error correction and apodization are considered. As a result, the transfer function of the spectrometer is calculated, and then the spectrum is reconstructed based on the relationship between the transfer function and the interferogram. The spectrometer comprises a modified Sagnac interferometer. The spectral reconstruction is conducted with a source with central wave number of 6,451 cm^{-1} and spectral width of 337 cm^{-1}. In a conventional Fourier-transform method the best spectral resolution is 27 cm^{-1}, but by means of the spectral reconstruction method the spectral resolution improved to 8.7 cm^{-1}, without changing the interferometric structure. Compared to a conventional Fourier-transform method, the spectral width in the reconstructed spectrum is narrower by 20 cm^{-1}, and closer to the reference spectrum. The proposed method allows high performance for static modulated Fourier-transform spectrometers.

Keywords : Interferometer, Reconstruction, Spectrometry, Static modulation
OCIS codes : (000.4430) Numerical approximation and analysis; (070.4790) Spectrum analysis; (120.3180) Interferometry; (300.6300) Spectroscopy, Fourier transforms

I. INTRODUCTION

A Fourier-transform spectrometer is extensively applicable in many scientific fields, due to its high throughput and multiplexing advantages, compared to diffractive optics-based spectroscopy [1]. In a Fourier-transform spectrometer an interferogram is obtained by modulating an optical-path difference, and a spectrum is obtained by performing a Fourier transform on the interferogram. In a conventional Fourier-transform spectrometer an interferogram can be obtained using an interferometric structure based on a Michelson interferometer, in which the optical-path difference is easily modulated by moving one of two mirrors back and forth. One severe disadvantage is that the spectrometer has to be operated under vibration-free conditions, or else errors occur from the incomplete optical alignment during mirror movement. Hence the spectrometer must be sophisticated, and as a result is bulky and expensive.

Various static modulation-based Fourier-transform spectrometers have been reported, to substitute for a conventional dynamic modulation-based Fourier transform spectrometer. Unlike the conventional type, they do not need mechanically movable components, and produce a spatially modulated optical-path difference from an interferometric structure, resulting in a compact spectrometer. Furthermore, this spectrometer is immune to vibration, allowing rapid measurement. A modified Sagnac interferometer [1–4], a Wollaston-prism-based interferometer [5–8], and a single-

*Corresponding author: jwk@hanseo.ac.kr, ORCID 0000-0003-1779-7987

Color versions of one or more of the figures in this paper are available online.

pISSN: 2508-7266 / eISSN: 2508-7274 https://doi.org/10.3807/COPP.2022.6.3.244

mirror-based interferometer [9] were introduced as sophisticated static modulation-based spectrometers. These spectrometers lead to a short maximum optical-path difference, because the value is limited by the interferometric structure. The number of sampling data points in the static modulation-based spectrometer is insufficient, because the total number of sampling points depends on the number of pixels in the overlapped sector of a detector in a one-dimensional array. As the result, static modulated Fourier-transform spectrometers have suffered from poor spectral resolution.

As a suggestion to overcome the poor spectral resolution, it is possible for the maximum optical-path difference to be increased out of necessity. Then it is suggested to add an extra optical component that modulates optical-path difference in two-dimensional space. An interferometer based on two birefringent prisms [10] and one based on two sets of stepped mirrors [11] were taken into account. Meanwhile, a long maximum optical-path difference was achieved by the wrapping method [12]. These studies were based on changing the physical structures, leading to complexity of the spectrometer. On the other hand, a signal-padding technique [13] improves the spectral resolution without changing the interferometer's structure. It works effectively even when the number of data points is insufficient.

A spectral reconstruction method was employed in a scalable Fourier transform spectrometer [14]. It consists of several optical switches. Since the optical-path difference increases exponentially with the number of optical switches, a long maximum optical-path difference was obtained with just a few optical switches and delays. However, the number of sampling points is related to the number of permutations of the switches, resulting in few sampling points and poor spectral resolution. The spectral reconstruction algorithm is effective to surpass these shortcomings. The spectrum is reconstructed by calculating the relationship of the interferogram and a transfer function. The transfer function is composed of signals measured through wavelength sweeping for each permutation of the optical switches. The reconstruction algorithm enables the spectrometer to achieve a spectral resolution that many static modulated Fourier-transform spectrometers cannot. However, to obtain a high spectral resolution, sufficient data points are needed in the given wavelength range. In the process of obtaining a transfer function this may be difficult to achieve, because the wavelength sweeping and phase errors should be precisely controlled and corrected respectively.

In the static modulated Fourier-transform spectrometer, although a long maximum optical-path difference may be obtained, high spectral resolution is still not obtainable, due to the limitation of the total sampling data points. In this paper, we propose a reconstruction algorithm to overcome these shortcomings. In the first place, we investigate how structural parameters such as the mirror displacement, optical-path difference, and focal length contribute to generating the transfer function of the spectrometer. Consequently the transfer function can be calculated over a wide spectral range, without the wavelength sweeping. We choose the elastic net, known as the most effective regression method. During spectral reconstruction, we empirically find that the information at high optical-path difference induces distortion. The phase error of the interferogram causes the zero-path difference to be shifted, resulting in mismatch of the zero-path difference between the interferogram and the transfer function. It also induces spectral distortion. We discuss applications of the apodization function to reduce the distortion, and an approach for compensating the phase mismatch.

The static modulated Fourier-transform spectrometer consists of a modified Sagnac interferometer, so the maximum optical-path difference and sampling frequency are easily adjusted by altering a mirror's position. It has the advantage of avoiding aliasing. A source with 6,451 cm^{-1} central wave number and 337 cm^{-1} spectral width is applied. Each set of interferogram and transfer function is determined for each pair of different positions of the mirror. The transfer function is calculated within the wave number range from 3,571 to 12,500 cm^{-1}, which is the same as the range of the detector and is much broader than other transfer functions produced by wavelength sweeping. The reconstruction is performed on each data set. Finally, the spectral resolution significantly improves from 27 cm^{-1} to 8.7 cm^{-1}, which is, to our knowledge, the best value among has ever reported in the static modulated Fourier-transform spectrometer system. This reconstruction algorithm enables the static modulated Fourier-transform spectrometer to exhibit high performance that the other types of static modulated Fourier-transform spectrometers cannot match.

II. METHODS

The modified Sagnac interferometer comprises one beam splitter and two mirrors. The beam splitter is tilted by 45°, and the two mirrors are tilted by 67.5° from the optical axis. Figure 1(a) shows the static modulated Fourier-transform spectrometer comprising the modified Sagnac interferometer, during the reconstruction process. The sample interferogram (SI) is observed by detector (D) and is sent to the computer interface (CI). The CI performs the phase correction on the interferogram, and creates the transfer function of the transfer-function matrix of the spectrometer (TM) to reconstruct the spectrum (RS). The reconstruction is conducted by elastic-net regression.

If M1 and M2 are located at equal distances from the beam splitter (BS), after the incident beam is split at the BS the resulting beams travel equal optical-path lengths, resulting in no optical-path difference between the two beams. Therefore, the interferogram cannot be formed in the focal plane where the one-dimensional detector D is placed. If M2 is moved by a from the initial symmetric position, each beam travels a different optical-path length. When both beams exit the interferometer, they are separated by dis-

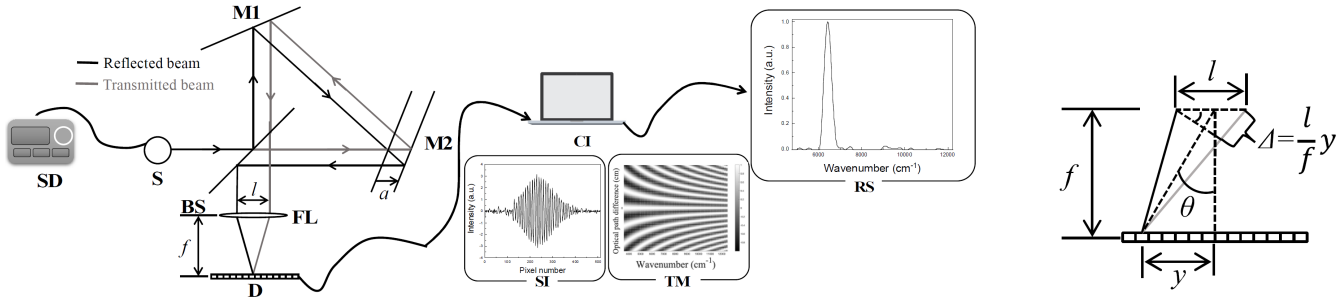

(a) (b)

FIG. 1. The static modulated Fourier-transform spectrometer during the reconstruction process and a magnified optical layout for its optical-path difference. (a) Schematic view of the static modulated Fourier-transform spectrometer consisting of a modified Sagnac interferometer. S, source; SD, source driver; M1, fixed mirror; M2, displaced mirror; BS, beam splitter; FL, focusing lens; D, one-dimensional detector; CI, computer interface; SI, sample interferogram; TM, transfer-function matrix of the spectrometer; RS, reconstructed spectrum. (b) Magnified optical layout near the one-dimensional detector array.

tance l. This distance is proportional to a and is expressed as [1, 13]

$$l = \sqrt{2}a, \tag{1}$$

where l is the separation of the two beams and a is the displacement of M2 from the symmetric position.

In the modified Sagnac interferometer, the optical-path difference in the focal plane is obtained from the optical layout shown in Fig. 1(b). If θ is small enough, the optical-path difference is expressed as [15]

$$\Delta = y\frac{l}{f}, \tag{2}$$

where Δ is the optical-path difference, y is the detector-surface-directional position in the focal plane (related to the pixel width of the detector), and f is the focal length of the lens. In the static modulated Fourier-transform spectrometer, the spectral resolution is inversely proportional to the maximum optical-path difference. The maximum optical-path difference depends on both the optical-path difference introduced in Eq. 2 and the overlapped sector width of two beams. If l is long, the optical-path difference is increased; then the width of the overlapped sector is reduced, so that the number of sampling data points in the overlapped sector is not sufficient to describe the spectrum. Owing to these reasons, the spectral resolution of the static modulated Fourier-transform spectrometer is limited.

Associated with the interferogram, the optical-path difference is expressed as

$$I(ny_{\min}) = \int B(\bar{\nu})\cos(2\pi\bar{\nu}(ny_{\min})\frac{l}{f})d\bar{\nu}, \tag{3}$$

where $I(ny_{\min})$ is the interferogram, $y_{\min}$ is the pixel width of the detector, n is an integer indicating pixel position, $B(\bar{\nu})$ is the spectral information, and $\bar{\nu}$ is the wave number. As a result, the obtained interferogram appears to be discrete, and since the spectrum is obtained from the Fourier transform, it is also discrete. The interferogram, the transfer function, and the spectral information compose a linear equation [14]

$$\mathbf{I} = \mathbf{TB}, \tag{4}$$

where $\mathbf{I}$ is the interferogram (a column vector with M elements), $\mathbf{B}$ is the spectral information (a column vector with N elements), and $\mathbf{T}$ is the transfer function of the spectrometer (an $M \times N$ matrix). If the inverse matrix of $\mathbf{T}$ exists and the interferogram is given, the spectral information is reconstructed. We assume that the cosine term in Eq. 3 is the transfer function of the spectrometer. In addition, we apply an apodization function to the transfer function, because the signal-to-noise ratio at high optical-path difference is so low that spectral distortion may result. In this study, the Blackman-Harris function among applicable apodization functions is applied, because it produces the smallest side lobes. The transfer function $\mathbf{T}$ is expressed as follows:

$$\mathbf{T} = \begin{bmatrix} BH(1)\cos(2\pi\bar{\nu}_1(1y)\frac{l}{f}) & \cdots & BH(1)\cos(2\pi\bar{\nu}_k(1y)\frac{l}{f}) \\ \vdots & \ddots & \vdots \\ BH(n)\cos(2\pi\bar{\nu}_1(ny)\frac{l}{f}) & \cdots & BH(n)\cos(2\pi\bar{\nu}_k(ny)\frac{l}{f}) \end{bmatrix}, \tag{5}$$

where $\bar{\nu}_1$ is the minimum wave number and $\bar{\nu}_k$ the maximum wave number. The wave-number range is given by that of the detector. $BH(n)$ is the Blackman-Harris function with 4-terms [16]. For the reconstruction, the number of wave-number components must be greater than the number of data points of the interferogram [14].

The obtained interferogram contains phase error, resulting in the zero-path differences being shifted. The mismatch of zero-path difference distorts the reconstructed spectrum. Fortunately, the phase information of the interferogram is reconstructed from the real and imaginary parts of the spectrum, and the error is then corrected by the Mertz phase correction. The phase information is reconstructed as [17]

$$\theta_{\bar{\nu}} = \frac{\mathrm{Im}[B(\bar{\nu})]}{\mathrm{Re}[B(\bar{\nu})]}, \tag{6}$$

where $\mathrm{Re}[B(\bar{\nu})]$ and $\mathrm{Im}[B(\bar{\nu})]$ are the real and imaginary parts of the spectrum respectively, and $\theta_{\bar{\nu}}$ is the phase as a function of the wave number. From the relationship between the magnitude spectrum and the complex spectrum, the phase-corrected spectrum is obtained as

$$B'(\bar{\nu}) = B(\bar{\nu})\mathrm{e}^{-i\theta_{\bar{\nu}}} = \mathrm{Re}[B(\bar{\nu})]\cos(\theta_{\bar{\nu}}) + \mathrm{Im}[B(\bar{\nu})]\sin(\theta_{\bar{\nu}}), \tag{7}$$

where $B'(\bar{\nu})$ is the phase-corrected spectrum that is equivalent to the magnitude spectrum. The phase-corrected interferogram is obtained from the inverse Fourier transform of the phase-corrected interferogram as

$$I'(ny) = \int B'(\bar{\nu}) e^{i2\pi\bar{\nu}(ny)l/f} d\bar{\nu}, \tag{8}$$

where $I'(ny)$ is the phase-corrected interferogram. Figure 2 shows the spectral reconstruction procedure in the static modulated Fourier-transform spectrometer. In advance, we would like to discuss how the spectrum is commonly obtained: The spectrum is obtained from the Fourier transform of the interferogram. Subsequently, phase correction is required to correct the phase error in the spectrum. The phase error occurs when the optical-path difference shifts [17]. A major drawback of this traditional procedure is poor spectral resolution, due to the tradeoff between the maximum optical-path difference and the width of the overlapped sector. The spectral reconstruction method is effective at overcoming the limitation due to this tradeoff. This method is applied when the inverse matrix of **T** exists in Eq. 4. The spectrum is numerically calculated using the standard linear-regression model given by [14, 18]

$$I = B_0 + \sum_{k=1}^{N} T_k B_k, \tag{9}$$

where I is the interferogram at one position in the focal plane, B_0 represents an error, k is an index representing the wave number, N is the number of wave-number elements, T_k is the transfer function of the spectrometer, and B_k represents the spectral information.

The estimation of the spectral information is conducted by minimizing the residual sum of squares [18]. The standard regression model has overfitting and bias problems. Ridge [19] and lasso [20] regressions are introduced for better estimation. Afterward, an elastic-net method with the help of both ridge and lasso is introduced [14, 18, 21, 22]. Equation (9) is rewritten as

$$\min_{B_0,B} = \frac{1}{2N}\sum_{n=1}^{M}(I_n - B_0 - \mathbf{T}_n^{\mathrm{T}}\mathbf{B})^2 + \lambda(+\alpha\|\mathbf{B}\|_1 + \frac{(1-\alpha)}{2}\|\mathbf{B}\|_2^2), \tag{10}$$

where M is the number of data points of the interferogram, I_n is the interferogram, n indicates the pixel position, $\mathbf{T}_n$ is the matrix for the transfer function of the spectrometer given by $\sum_{k=1}^{N} T_{n,k}$, **B** is the spectral information given by $\sum_{k=1}^{N} B_k$, and λ is a positive regularization parameter. The parameter λ is basically determined by a standard holdout cross-validation technique [14, 21]. α is the value that defines the ratio of lasso regression to ridge regression. If α is 1, Eq. 10 becomes lasso regression. $\|\mathbf{B}\|_1$ and $\|\mathbf{B}\|_2^2$ are given by $\sum_{k=1}^{N}|B_k|$ and $\sum_{k=1}^{N}B_k^2$, respectively.

III. RESULTS AND DISCUSSION

The spectrometer is built as shown in Fig. 1. As the incident source, an light-emitting diode (LED) with center wavelength of 6451 cm^{-1} and output of 2 mW is used. A parabolic mirror-based reflector is coupled to the LED to generate a parallel beam. A thermal electric module is used to control the temperature of the LED to be 25 ℃. The beam diameter is 8.23 mm, based on the width of the e^{-2} point from the highest intensity. Two silver-coated mirrors are used, in which each width is 2 inches. The beam splitter has 50% transmittance at 45°-to-incident angles, in the wavelength range from 3,920 to 11,110 cm^{-1}. The sensing length and pixel pitch of the detector are 12.8 mm and 25 μm respectively. The exposure time is set to 4 ms. For comparison, the spectrum of the source is separately measured by a monochromator.

Figure 3 shows the transfer function of the spectrometer. It is created using Eq. 5. The spectral range is from 3,571 cm^{-1} to 12,500 cm^{-1}, which coincides with that of the detector. In the reconstruction process, the spectral resolution is related to the interval between the wave-number components in the transmission spectrum. With the consideration that the number of wave-number components must be

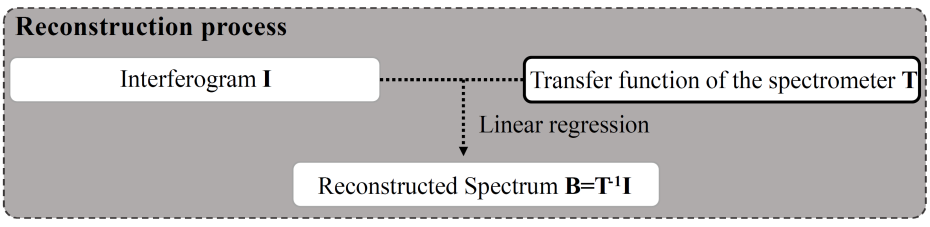

FIG. 2. Spectral reconstruction procedure.

greater than the number of data points in the interferogram, we choose 1,024 data points. In this case the spectral resolution is 8.7 cm^{-1}. In our previous study [13], the best spectral resolution was theoretically calculated to be 27 cm^{-1}, so the spectral resolution in this study has improved by 70%.

The zero-path difference of the transfer function is located at the center of the focal plane. The recorded interferogram contains a phase error, resulting in a slightly shifted zero-path difference. The difference between the transfer function and the interferogram leads to an inaccurately reconstructed spectrum. Figure 4(a) shows a comparison of the interferogram to the transfer function. This transfer function is calculated by the sum of the wave numbers along with each optical-path difference. At the zero-path difference the transfer function has the highest intensity, whereas in the case of the interferogram the highest intensity does not appear at the zero-path difference. The phase in the interferogram is reconstructed using Eq. 6, and then the error is corrected with Eq. 7. Figure 4(b) shows a comparison of the phase-corrected interferogram to the transfer function. The highest intensity appears at the center, in both the interferogram and the transfer function.

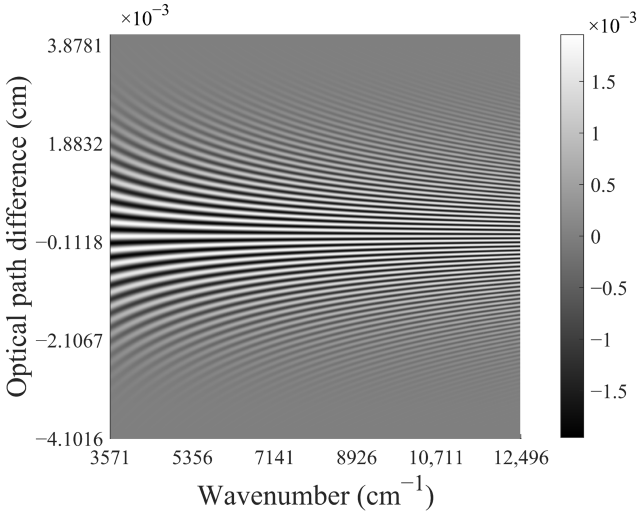

FIG. 3. Transfer function of the spectrometer, when the displacement of the mirror is 2 mm. The spectral range is from 3,571 cm^{-1} to 12,500 cm^{-1}.

Figure 5 shows the changes of the reconstructed spectra under the applied apodization. The reconstruction is performed using Eq. 10. The solid line is the reconstructed spectrum without applying the apodization function; the dashed line is the reconstructed spectrum with applying the apodization function. The Blackman-Harris function strongly suppresses the side lobes in the spectrum, and converts values into positive ones on the spectrum. The interferograms are obtained at different optical-path differences, evaluating the transfer function of the spectrometer. Figure 5(a) shows the reconstructed spectrum for 2 mm of mirror displacement. The spectral width of the reconstructed spectrum is 479 cm^{-1} when the apodization function is not applied. Subsequently, the reconstruction is conducted after the apodization function has been applied. The spectral width is reduced to 400 cm^{-1}. The spectral width of the source measured by the monochromator is 337 cm^{-1}. The spectral-width difference between the reference and reconstructed spectra is significantly reduced, from 142 cm^{-1} to 63 cm^{-1}, but the reduced spectral width is still wider than that of the reference spectrum, as expected for the relatively short maximum optical-path difference. Figure 5(b) shows the reconstructed spectrum for 5 mm of mirror displacement. The spectral widths are both close to 356 cm^{-1}. However, a severe spectral distortion is observed around 6450 cm^{-1} when the apodization function is not applied. By ap-

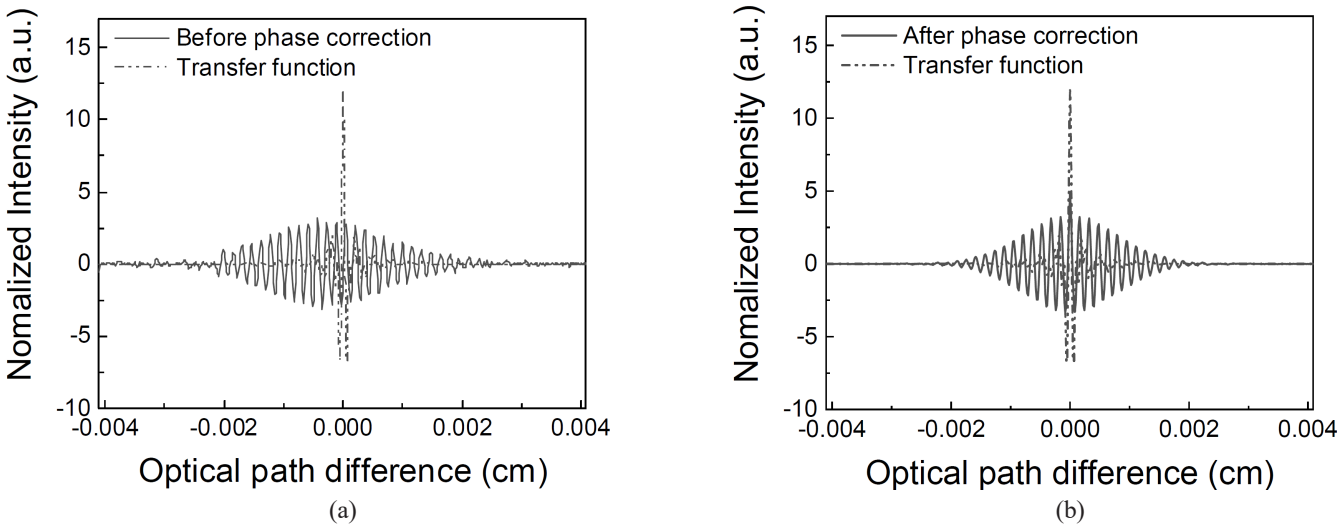

FIG. 4. Effectiveness of phase correction on the interferogram, compared to the transfer function. (a) Phase not corrected, and (b) corrected interferogram. The transfer function is calculated as the sum of the wave-number components in the transfer function along the optical-path difference. The interferogram and transfer function are obtained at 2 mm of mirror displacement.

plying the apodization function to the transfer function, the spectrum is successfully reconstructed.

Figure 6(a) shows the spectrum for 2 mm of mirror displacement. The true spectrum (dashed line) is that obtained by the formal Fourier-transform process, without the reconstruction process. The reconstruction (solid line) is the spectrum obtained by the regression of Eq. 10. The reference (dotted line) is the spectrum obtained by the monochromator. The spectral width of the source obtained by the formal Fourier-transform procedure is 488 cm^{-1}, and the spectral resolution is 122 cm^{-1}. The spectral width of the source reconstructed by Eq. 10 is 400 cm^{-1}, and the spectral resolution is 8.7 cm^{-1}. This reconstructed spectrum is more precise than the reference spectrum, when λ and α are 5.0 and 0.75 respectively. The spectral width of the source on the monochromator is 337 cm^{-1}. Compared to the reference spectrum, the spectral widths of both the reconstructed spectrum and the spectrum obtained by Fourier transform are broad. This is expected, due to the short maximum optical-path difference. Figure 6(b) shows the spectrum for 5 mm of mirror displacement. In general, the maximum optical-path difference depends on the overlapped sectors. For long mirror displacement, the short width of the overlapped sector exists, so the maximum optical-path difference is limited. In this experiment, the optimal mirror displacement that maintains the longest maximum optical-path difference is 5 mm. The spectral width of the source from the formal Fourier-transform procedure is 376 cm^{-1}, and the spectral

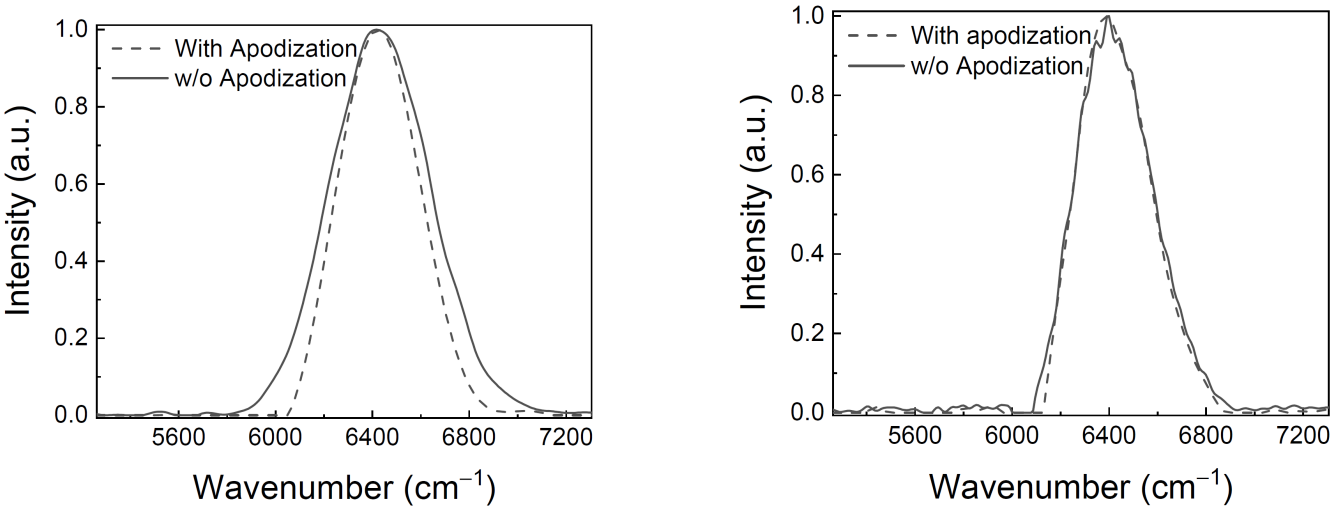

FIG. 5. Change in the reconstructed spectrum, with and without apodization of to the transfer function. The spectrum is obtained at (a) 2 mm of mirror displacement and (b) 5 mm of mirror displacement.

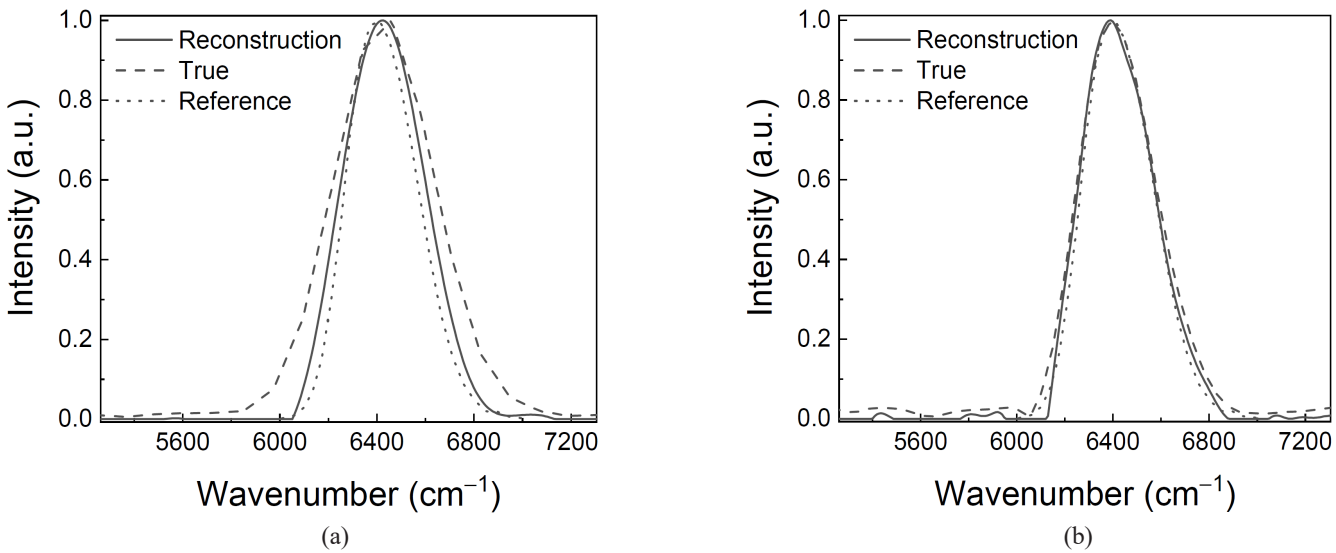

FIG. 6. Spectrum comparison. The spectrum was obtained at (a) 2 mm of mirror displacement, and (b) 5 mm of mirror displacement.

resolution is 49 cm^{-1}. However, when the reconstruction process is applied, the spectral width of the source reconstructed by Eq. 10 and the spectral resolution improve to 356 cm^{-1} and 8.7 cm^{-1} respectively. In this case, the values of λ and α applied in the calculation are 3.4 and 0.75 respectively. The difference in spectral width between the reference and reconstructed spectra, compared to the spectral width of 63 cm^{-1} in the case of 2-mm mirror displacement, is significantly reduced to 19 cm^{-1}. These results assume that it is still important to obtain a long maximum optical-path difference for better reconstruction of the spectrum. In addition, comparing the spectral width of the reconstructed spectrum to that of the spectrum obtained simply by Fourier transform, the spectral width is as narrow as 20 cm^{-1}, which is much closer to that of the reference spectrum. We can perform the reconstruction of a wider spectrum [14] and achieve a higher spectral resolution of 8.7 cm^{-1} [13].

IV. CONCLUSION

The elastic-net reconstruction algorithm was introduced for the static modulated Fourier-transform spectrometer. The algorithm successfully reconstructed the spectrum of the broad spectral band. In this study, the transfer function of the spectrometer was generated in matrix form. The optical-path difference and the interferogram in the focal plane were discussed, to create the transfer function for the static modulated Fourier-transform spectrometer, which consisted of a modified Sagnac interferometer. To successfully reconstruct the spectrum, the phase error of the interferogram had to be corrected. The Mertz phase-correction method was effective for compensating the error. In addition, an apodization function was employed to suppress the distortion of the reconstructed spectrum. The wave-number range was set to be equal to the measurable range of the detector. The spectral resolution depended on the interval between wave-number components in the transfer function. The number of wave-number components was chosen to be greater than that of the interferogram. For better reconstruction, the acquisition of the longest maximum optical-path difference was important. Compared to the spectral resolution in the formal Fourier-transform procedure, the suggested approach enabled the spectrometer to significantly improve the spectral resolution.

FUNDING

National Research Foundation of Korea (NRF-2020R1A6A3A01099403); National Research Foundation of Korea (NRF-2021R1I1A3052065).

ACKNOWLEDGMENT

We thank the anonymous referees for their useful suggestions.

DISCLOSURES

The authors declare no conflicts of interest.

DATA AVAILABILITY

Data underlying the results presented in this paper are not publicly available at this time of publication, which may be obtained from the authors upon reasonable request.

REFERENCES

1. T. Okamoto, S. Kawata, and S. Minami, "Fourier transform spectrometer with a self-scanning photodiode array," Appl. Opt. **23**, 269–273 (1984).
2. Y. Ferrec, J. Taboury, H. Sauer, and P. Chavel, "Compactness of lateral shearing interferometers," Appl. Opt. **50**, 4656–4663 (2011).
3. J. He and Q. Zhang, "Design and analysis of a modified Sagnac interferometer for upper atmospheric wind measurement," Optik **124**, 2658–2660 (2013).
4. S. Chatterjee and Y. P. Kumar, "White light differential interference contrast microscope with a Sagnac interferometer," Appl. Opt. **53**, 296–300 (2014).
5. M. J. Padgett and A. R. Harvey, "A static Fourier-transform spectrometer based on Wollaston prisms," Rev. Sci. Instrum. **66**, 2807–2811 (1995).
6. X. Lin, F. Zhou, H. Li, and H. B. Zhao, "Static Fourier-transform spectrometer based on Wollaston prism," Optik **125**, 3482–3484 (2014).
7. Q. Liu, C. Bai, J. Liu, J. He, and J. Li, "Fourier transform imaging spectropolarimeter using ferroelectric liquid crystals and Wollaston interferometer," Opt. Express **25**, 19904–19922 (2017).
8. J. Réhault, R. Borrego-Varillas, A. Oriana, C. Manzoni, C. P. Hauri, J. Helbing, and G. Cerullo, "Fourier transform spectroscopy in the vibrational fingerprint region with a birefringent interferometer," Opt. Express **25**, 4403–4412 (2017).
9. M. Schardt, P. J. Murr, M. S. Rauscher, A. J. Tremmel, B. R. Wiesent, and A. W. Koch, "Static Fourier transform infrared spectrometer," Opt. Express **24**, 7767–7776 (2016).
10. J. Li, C. Qu, H. Wu, and C. Qi, "Spectral resolution enhanced static Fourier transform spectrometer based on a birefringent retarder array," Opt. Express **27**, 15505–15517 (2019).
11. M. H. Kőhler, M. Schardt, M. Műller, P. Kienle, K. Wang, X. Dong, C. Giebeler, B. R. Wiesent, M. Jakobi, and A. W. Koch, "Static Fourier transform mid-infrared spectrometer with increased spectral resolution using a stepped mirror," OSA Continuum **3**, 2134–2142 (2020).
12. A. Watanabe and H. Furukawa, "High-resolution and high-throughput multichannel Fourier transform spectrometer with two-dimensional interferogram warping compensation," Opt. Commun. **413**, 8–13 (2018).
13. J. Y. Cho, S. H. Lee, and W. K. Jang, "Improvement of spectral resolution by signal padding method in the spatially modulated Fourier transform spectrometer based on a Sagnac interferom-

eter," Appl. Opt. **58**, 6755–6761 (2019).
14. D. M. Kita, B. Miranda, D. Favela, D. Bono, J. Michon, H. Lin, T. Hu, and J. Hu, "High-performance and scalable on-chip digital Fourier transform spectroscopy," Nat. Commun. **9**, 4405 (2018).
15. M.-L. Junttila, J. Kauppinen, and E. Ikonen, "Performance limits of stationary Fourier spectrometers," J. Opt. Soc. Am. A **8**, 1457–1462 (1991).
16. F. J. Harris, "On the Use of Windows for Harmonic Analysis with the Discrete Fourier transform," Proc. IEEE **66**, 51–83 (1978).
17. K. Rahmelow and W. Hübner, "Phase correction in Fourier transform spectroscopy: subsequent displacement correction and error limit," Appl. Opt. **36**, 6678–6686 (1997).
18. H. Zou and T. Hastie, "Regularization and variable selection via the elastic net," J. R. Stat. Soc. B **67**, 301–320 (2005).
19. A. Hoerl, and R. Kennard, "Ridge regression," in *Encyclopedia of Statistical Sciences*, S. Kotz, C. B. Read, N. Balakrishnan, B. Vidakovic, and N. L. Johnson, Eds., (John Wiley & Sons, USA, 2004).
20. R. Tibshirani, "Regression shrinkage and selection via the lasso," J. R. Stat. Soc. B **58**, 267–288 (1996).
21. S. S. Shai and B. D. Shai, *Understanding Machine Learning: From Theory to Algorithms* (Cambridge University Press, Cambridge, UK, 2014), Chapter 11.
22. J. Friedman, T. Hastie, and R. Tibshirani, "Regularization paths for generalized linear models via coordinate descent," J. Stat. Softw. **33**, 1–22 (2010).